Thermopower in oxide heterostructures: The importance of being multiple-band conductors

A. Filippetti,[1] P. Delugas,[1] M. J. Verstraete,[2] I. Pallecchi,[3] A. Gadaleta,[3] D. Marré,[3] D. F. Li,[4] S. Gariglio,[4] and V. Fiorentini[5]

[1]*CNR-IOM, UOS Cagliari, S.P. Monserrato-Sestu Km. 0.700, Monserrato (CA), Italy*

[2]*Département de Physique, B5a, Université de Liège, B-4000 Sart-Tilman, Belgium*

[3]*CNR-SPIN UOS Genova and Dipartimento di Fisica, Via Dodecaneso 33, 16146 Genova, Italy*

[4]*DPMC, University of Geneva, 24 Quai Ernest-Ansermet, 1211 Genève 4, Switzerland*

[5]*CNR-IOM, UOS Cagliari and Dipartimento di Fisica, Université di Cagliari, Monserrato (CA), Italy*

(Received 14 February 2012; revised manuscript received 12 October 2012; published 5 November 2012)

We combine transport experiments, advanced *ab initio* calculations, and model analysis to determine the thermoelectric power in the two-dimensional electron gas formed at the paradigmatic oxide interface $SrTiO_3/LaAlO_3$. We demonstrate that contrary to popular expectation, quantum confinement does not enhance the thermoelectric power of the electron gas at this interface with respect to its corresponding three-dimensional case. Our analysis directly relates the thermopower behavior to band structure characteristics typical of the oxide heterostructure (i.e., on-site and intersite band splitting), furnishing general interpretive prescriptions to search for oxide heterostructures with improved thermoelectric capabilities.

DOI: 10.1103/PhysRevB.86.195301 PACS number(s): 73.20.At, 73.40.Lq, 73.50.Lw, 73.63.Hs

I. INTRODUCTION

Materials with large thermoelectric power, capable to efficiently convert temperature gradients into electric power (Seebeck effect) or magnetization (spin-Seebeck), furnish in principle the cleanest and most straightforward way to produce electrical power from heating or, vice versa, heating and cooling from an electrical source, thus opening new possibilities in terms of recycling waste energy and reducing power consumption.

Alas, practical applications based on thermoelectric conversion have been limited, so far, by the relatively low efficiency (quantified by the so-called figure of merit $Z = \sigma S^2/k$, where S, σ, and k are thermopower, electrical, and thermal conductivity) of thermoelectric devices with respect to conventional mechanical systems for cooling and heating. However, the observation of enhanced thermopower in low-dimensional materials (with the adimensional ZT factor larger than the $ZT = 1$ threshold of interest)[1,2] opens up entirely new perspectives for thermoelectric conversion technology and its potential applications in energy harvesting and new heating/cooling devices. Thermopower enhancement by quantum confinement was first predicted by early models[3–7] and then observed in some Te-based alloy heterostructures (Bi_2Te_3/Sb_2Te_3 superlattices;[8] PbTe/PbSeTe and PbTe/PbSnSeTe quantum dot superlattices[9]) which however remain unappealing in practice, due to the toxicity of heavy metals which are volatile at growth temperatures of about 1000 K (the use of heavy ions is key to the idea of increasing Z by reducing the thermal lattice conductivity k). More recently, great excitement was provoked by the observation of enhanced thermopower in Nb-doped $SrTiO_3$(STO)-based heterostructures[10–13] with measured thermopower up to five times larger than the STO bulk value, and an estimated ZT larger than 2.

The net effect of charge confinement on the thermoelectric efficiency is not easy to grasp and predict, since it may depend on several conflicting mechanisms, such as phonon-phonon scattering (which reduces k and then increases ZT) and electron-phonon scattering (which reduces S and σ). In our analysis we leave aside these scattering processes, and only focus on the purely electronic mechanism acting on the Seebeck and the electric conductivity in lower dimensionality.

The primary source typically invoked to motivate the expected increase of thermopower with charge confinement is the rise of charge density slope at the Fermi energy $(\partial n/\partial\epsilon)_{\epsilon_F}$. Thermopower and charge density are related by the popular Cutler-Mott formulas[14]

$$S = \frac{\pi^2 k_B^2 T}{3e}\left(\frac{\partial \ln\sigma(\epsilon)}{\partial\epsilon}\right)_{\epsilon_F}, \quad \sigma(\epsilon) = en(\epsilon)\mu(\epsilon)k_B T, \quad (1)$$

where $\sigma(\epsilon)$, $\mu(\epsilon)$, and $n(\epsilon)$ are spectral conductivity, mobility, and density of states (DOS), respectively. However, we should notice that the increase of $(\partial n/\partial\epsilon)_{\epsilon_F}$ becomes obvious only in the case of a single-band conductor. For multiband systems such as oxide heterostructures, the effects of quantum confinement on the density of states may be much more complicated. Furthermore, a peaked DOS may be the signature of electron correlation, which can in turn lower the electron mobility. These considerations point to the fact that, unless we are in the presence of a simplistic single-band system, qualitative predictions may be faulted, and a reliable determination of thermopower in oxide heterostructures necessarily requires a rigorous account of the electronic properties, possibly by *ab initio* calculations.

A technologically important case study to investigate the effects of the multiband character on the thermopower behavior is the much celebrated $SrTiO_3/LaAlO_3$ (STO/LAO) interface,[15–18] the foremost candidate material as building block of future oxide-based nanotechnology. While electronic,[19–23] structural,[24–26] transport,[27,28] and magnetotransport[29–34] properties for STO/LAO have been thoroughly analyzed, its thermoelectric behavior is comparatively less known. Some of us[35] have recently delivered thermopower measurements for several STO/LAO samples, showing, somewhat unexpectedly, a lack of enhancement with respect to the n-doped STO bulk samples.

In this work we explain these observations from a fundamental viewpoint, providing a detailed analysis of the thermoelectric properties of this system and a close comparison

between interface and bulk samples. In particular, it will be demonstrated that the lack of thermopower enhancement with respect to the STO bulk at equivalent doping is related to the specific features of the interface electronic structure (on-site and intersite band splitting), which play against the increase of thermopower.

The mansucript is organized as follows: in Sec. II we describe the experimental setting and the theoretical methods; in Sec. III we display our results for the STO/LAO electronic structure (Sec. III A) and thermopower (Sec. III B); in Sec. IV we discuss our results, and finally in Sec. V we draw our conclusions.

II. METHODS

A. Experiment

The STO/LAO interface was deposited by pulsed laser deposition at a substrate temperature of 800 °C in an oxygen pressure of 10^{-4} mbar. After the growth, the sample was kept at 550 °C in 0.2 mbar of oxygen for one hour before the cooldown.[36]

Transport properties (resistance and Hall effect) are measured in a commercial PPMS system by Quantum Design in magnetic fields up to 9 T in the temperature range from 5 K to room temperature. The Seebeck coefficient was measured in a homemade apparatus by an ac technique. Commercially available Nb-doped $SrTiO_3$ single crystals were used to measure the bulk Seebeck coefficient in both the homemade apparatus and a PPMS system by Quantum Design.

B. Bloch-Boltzmann theory

The first-principles band structures were obtained by the Variational Pseudo-Self Interaction Correction (VPSIC) approach[37] and reported in detail in Ref. 38. The bands are used as input for Bloch-Boltzmann (BB) calculation[39,40] of thermopower (i.e., Seebeck coefficient S) and conductivity (σ) tensors (here only the interface-parallel diagonal components S_j and σ_j, with $j = x$ or y, are considered). For a $\mathcal{N}$-band system, S_j can be expressed as an average of band contributions:

$$S_j = \frac{1}{\mathcal{N}} \sum_{n=1}^{\mathcal{N}} S_{nj} = \frac{1}{\mathcal{N}\sigma_j} \sum_{n=1}^{\mathcal{N}} \Lambda_{nj}, \tag{2}$$

where $S_{nj} = \Lambda_{n,j}/\sigma_j$, and the total conductivity σ_j is a sum of individual band conductivities σ_{nj}. In BB theory,

$$\Lambda_{nj} = -\frac{e\mathcal{N}}{VT} \int d\mathbf{k}\, \tau_{n\mathbf{k}} \left(-\frac{\partial f}{\partial \epsilon_{n\mathbf{k}}}\right) (\epsilon_{n\mathbf{k}} - \mu)\, v_{jn\mathbf{k}}^2, \tag{3}$$

$$\sigma_{nj} = \frac{e^2}{V} \int d\mathbf{k}\, \tau_{n\mathbf{k}} \left(-\frac{\partial f}{\partial \epsilon_{n\mathbf{k}}}\right) v_{jn\mathbf{k}}^2, \tag{4}$$

where V is the volume, f the Fermi occupancy, μ the chemical potential, and v_j the Fermi velocity. The integrals are calculated by k-space interpolation of *ab initio* band energies. The usual assumption of a constant relaxation time is insufficient for a quantitative comparison with experiment. To overcome this limitation we use the simple analytic energy-dependent model:[41]

$$\tau(T,\epsilon) = F(T) \left(\frac{\epsilon - \epsilon_0}{K_B T}\right)^{\lambda}, \tag{5}$$

where ϵ_0 the conduction band bottom and λ depends on the dominant scattering mechanism (we fix $\lambda = 3/2$ suited for ionized impurity scattering). In the Seebeck expression the temperature-dependent prefactor cancels out, and the dependence on λ is rather weak, so we can consider the calculated Seebeck as substantially parameter-independent. On the other hand, the electric conductivity depends crucially on the model parameters. For our calculations of σ we have taken $F(T) = \tau_{\rm ref}(T_{\rm ref}/T)^{\lambda}$, where $\tau_{\rm ref}$ is a suitable reference value at temperature $T_{\rm ref}$, and $\tau_{\rm ref} = 3$ fs at $T_{\rm ref} = 20$ K for both bulk STO and STO/LAO. We have tested the accuracy of this expression for the relaxation time using the electron-doped STO bulk as a benchmark,[42,43] for which several sets of experimental data for Seebeck and dc conductivity exist in the literature. We have obtained a nice agreement with our calculated values in a wide range of doping and temperatures, not only for the Seebeck but even for the parameter-dependent electric conductivity.

C. Multiband effective mass model

In order to disentangle the contribution of individual bands to S and σ, we can exploit an effective Ti t_{2g} multiband model (a precursor for bulks can be found in Ref. 44) $\epsilon_{\nu\alpha\mathbf{k}} = \epsilon^0_{\nu\alpha} + (\hbar^2/2)({k_x}^2/m^*_{\alpha,x} + {k_y}^2/m^*_{\alpha,y} + {k_z}^2/m^*_{\alpha,z})$, where the band index $n \equiv (\nu,\alpha)$ is decomposed into a site index ($\nu = 1$ for the interface Ti, $\nu = 2$ for the second Ti from the interface, and so on), and $\alpha \equiv (d_{xy},d_{xz},d_{yz})$ labeling the t_{2g} orbitals.

Using this band parametrization, for a given $\nu\alpha$ band and current direction $j = x$ we obtain

$$\sigma_{\nu\alpha j} = e^2\beta\, C_{\alpha j} \int_{\epsilon^0_{\nu\alpha}}^{\infty} d\epsilon\, \tau(\epsilon) \left(-\frac{\partial f}{\partial \epsilon}\right) \left(\epsilon - \epsilon^0_{\nu\alpha}\right)^{1+\eta},$$

$$\Lambda_{\nu\alpha j} = -\frac{e\beta\mathcal{N}}{T} C_{\alpha j} \int_{\epsilon^0_{\nu\alpha}}^{\infty} d\epsilon\, \tau(\epsilon) \left(-\frac{\partial f}{\partial \epsilon}\right) (\epsilon - \mu)\left(\epsilon - \epsilon^0_{\nu\alpha}\right)^{1+\eta},$$

and for the corresponding band occupancy

$$P_{\nu\alpha} = \tilde{C}_{\alpha} \int_{\epsilon^0_{\nu\alpha}}^{\infty} d\epsilon\, f(\epsilon)\left(\epsilon - \epsilon^0_{\nu\alpha}\right)^{\eta}.$$

In three dimensions, $\eta = 1/2$, $C_{\alpha j} = (\sqrt{2}/\pi^2\hbar^3)\sqrt{m^*_{\alpha,x}m^*_{\alpha,y}m^*_{\alpha,z}}/m^*_{\alpha,j}$, and $\tilde{C}_{\alpha} = (\sqrt{2}V/\pi^2\hbar^3)\sqrt{m^*_{\alpha,x}m^*_{\alpha,y}m^*_{\alpha,z}}$. In two dimensions, $\eta = 0$, $C_{\alpha j} = (1/\pi\hbar^2 L)\sqrt{m^*_{\alpha,x}m^*_{\alpha,y}}/m^*_{\alpha,j}$, and $\tilde{C}_{\alpha} = (A/\pi\hbar^2)\sqrt{m^*_{\alpha,x}m^*_{\alpha,y}}$. $A = 15.467$ Å^2 is the 1×1 interface area; $V = A \cdot L$ is the supercell volume. The band sheet density is $n_{s,\nu\alpha} = P_{\nu\alpha}/A$ and the three-dimensional (3D) -equivalent band density $n_{\nu\alpha} = P_{\nu\alpha}/V$. The total conductivity and charge are then given by

$$\sigma_j = e^2\beta \int_{-\infty}^{\infty} d\epsilon\, \tau(\epsilon) \left(-\frac{\partial f}{\partial \epsilon}\right) \sum_{\nu\alpha} \Theta(\epsilon - \epsilon^0_{\nu\alpha}) C_{\alpha j} \left(\epsilon - \epsilon^0_{\nu\alpha}\right)^{1+\eta},$$

$$Q = \int_{-\infty}^{\infty} d\epsilon\, f(\epsilon) \sum_{\nu\alpha} \Theta\left(\epsilon - \epsilon^0_{\nu\alpha}\right) \tilde{C}_{\alpha j} \left(\epsilon - \epsilon^0_{\nu\alpha}\right)^{\eta},$$

where Θ is the step function (0 or 1 for negative or positive values, respectively). The total S is given by Eq. (2).

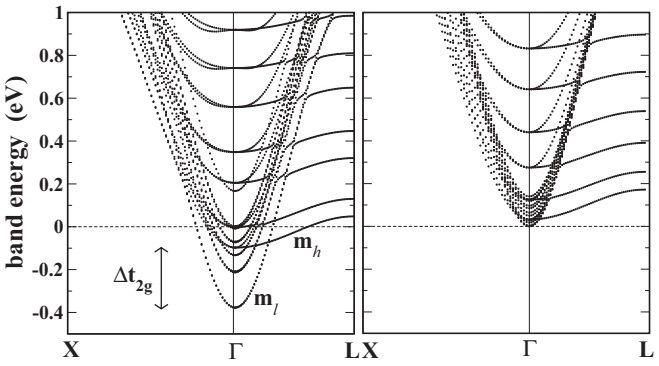

FIG. 1. Calculated STO/LAO Ti t_{2g} bands for (left) the metallic, fully compensated interface (charged by $Q = 1/2$ el/unit area, equivalent to $n_s = 3.2 \times 10^{14}$ cm^{-2}), and (right) the undoped, insulating interface. They represent two physical situations of a LAO thickness larger and smaller, respectively, than the threshold value necessary for the occurrence of the insulating metal transition. The zero is set to the Fermi energy on the left and to the band bottom on the right. Δt_{2g} is the on-site $d_{xy} - (d_{xz},d_{yz})$ orbital splitting, $m_l = 0.7m_e$, and $m_h = 8.8m_e$ light and heavy electron masses.

III. RESULTS

A. STO/LAO electronic properties

There is large consensus[45] on the fact that the characteristics of 2DEG observed at the STO/LAO interface differ remarkably from that found in conventional semiconductor interfaces. The latter is typically interpreted as a nearly-free electron gas enclosed within a wide box of some hundreds of nm, whose confinement is essentially governed by long-range electrostatics. At variance, most observations and first-principles calculations[38,46] coherently attest that the 2DEG in STO/LAO is tightly confined within a few nm from the interface, and distributed within a short series of adjacent, Ti-centered quantum wells, each of them one-cell wide. This atomic well-shaped confining potential is largely a characteristic of the chemical nature of the 3D t_{2g} states, which host the charge transferred from the LAO surface to the interface as a consequence of the Zener breakdown.

Here we specifically consider the band structure calculations[38] carried out by the VPSIC method,[37] which is capable of correcting the band-gap errors of standard density functional approaches, and then it correctly describes the band alignment at the interface. A detail of the VPSIC-calculated bands is reported in Fig. 1.

To understand the peculiarity of the 2DEG observed in STO/LAO, it is important to point out that even for STO bulk the t_{2g} masses are not isotropic: our calculations give $m^*_{xy,j} = (0.7,0.7,8.8)$, $m^*_{xz,j} = (0.7,8.8,0.7)$, and $m^*_{yz,j} = (8.8,0.7,0.7)$. At the interface, the orthogonal effective mass diverges, while the planar components are substantially unchanged. It follows that while d_{xy} remains essentially bulklike and almost unaware of the presence of the interface, the (d_{xz},d_{yz}) doublet suffers a large increase of electrostatic repulsion due to the collapse of the orthogonal spread. As a consequence there is a singlet-doublet on-site splitting which grows progressively with the amount of charge confined at the interface. In addition, an intersite Ti t_{2g} splitting is produced by the surface-to-interface charge transfer, which leaves the LAO film uncompensated and positively charged, resulting in an attractive electrostatic potential which lowers the Ti t_{2g} band energies closer to the interface with respect to the inner Ti t_{2g} bands of the substrate. As clearly visible in Fig. 1, the amplitude of the on-site and intersite splitting crucially depends on the amount of the electron charge trapped at the interface: at full compensation (when the $1/2$ electron per unit area equal to $n_s \sim 3.2 \times 10^{14}$ cm^{-2} needed to cancel the electric field in LAO is transferred to the interface), Δt_{2g} is large (350 meV on the first Ti) and the d_{xy} bands then capture most (about 70%) of the charge distributed in the first 5–6 Ti layers from the interface. Moving away from the interface, the on-site splitting is progressively reduced, until it closes up, and the charge starts to spill over into the d_{xz} and d_{yz} bands as well. However, at low charge concentration (such as $n_s \sim 10^{13}$ cm^{-2} typically measured in Hall experiments) the band structure corresponding to the insulating case (where Δt_{2g} is only 28 meV) may be closer to the actual experimental situation than the fully compensated case. In what follows we show that, in multiband systems, transport and thermoelectric properties crucially depend on the band alignment; thus the rigid band approximation (RBA) applied to the properties of the STO/LAO interface may give a substantial deviation from the experiment, which needs to be quantified.

B. STO/LAO thermopower and dc conductivity

Measurements and calculations for Seebeck and dc resistivity are reported in Fig. 2 for a STO/LAO sample with 5 LAO unit cells and Hall-measured $n_s = 2.4 \times 10^{13}$ cm^{-2}. As a reference, values for several Nb-doped STO bulk samples at different doping concentrations n_{3D} are reported as well. As expected, S increases (in modulus) with temperature, and decreases with doping concentration. For the STO bulk, the agreement between measured and calculated Seebeck is quite satisfying. The matching is more problematic for the STO/LAO interface: besides the deep phonon-drag peak in S measured for STO/LAO in the low-T region (which is not included in our BBT theoretical implementation) the major theoretical uncertainty is related to the RBA which, as previously discussed, may result in a substantial error bar on the calculated 2DEG properties. We can quantify this error bar considering two different "starting points" (shown in Fig. 1): the undoped insulating interface ($2DEG_0$) and the fully compensated interface ($2DEG_{1/2}$). Values of S and ρ for these two cases are respectively upper and lower bounds of the theoretical determination (this will be shown explicitly later on, with the band splitting analysis).

Now, we come to the comparison between STO and STO/LAO. Clearly, this is not straightforward: the Hall experiment directly measures the sheet density charge $n_s = n_{3D}L$ (i.e., the density integrated over the 2DEG extension L orthogonal to the interface) via the relation $n_s = -(I \cdot B)/V_H$ (where I, B, and V_H are the current, applied magnetic field, and Hall voltage, respectively), and the determination of the equivalent-doping 3D charge density n_{3D} requires the estimation of L, which is hard to achieve precisely. Indirect estimates obtained by fitting optical or transport measurements to simplified models report a scattered range of values from

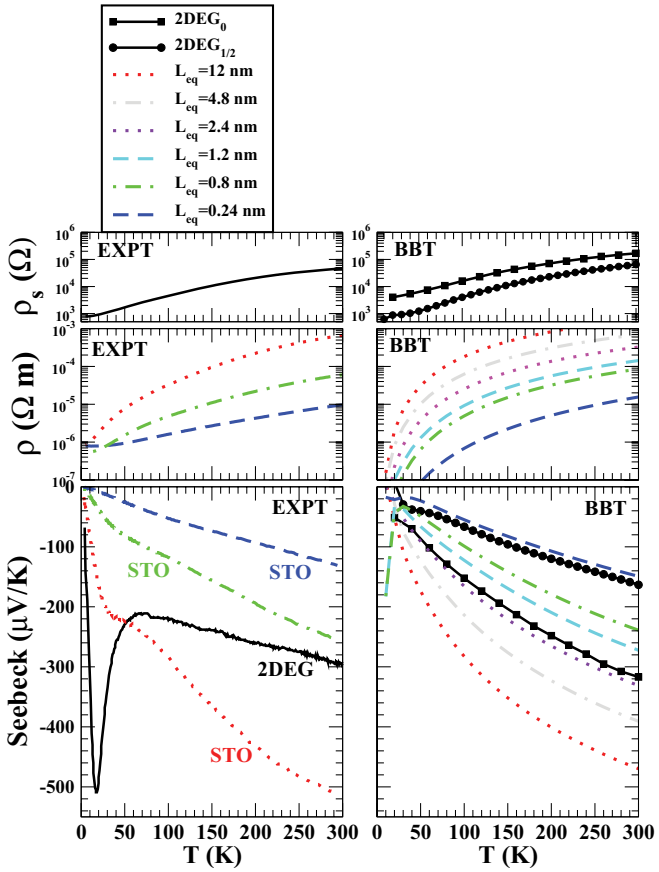

FIG. 2. (Color online) 2DEG sheet resistivity (ρ_s), STO bulk resistivity (ρ), and Seebeck coefficient (S) measured (EXPT, left panels) and calculated (BBT, right) for a 5 u.c. STO/LAO interface (solid black lines) and several n-doped STO bulk samples. The Hall-measured concentrations are $n_s = 2.4 \times 10^{13}$ cm^{-2} for the STO/LAO sample and $n_{3D} = 10^{21}$ cm^{-3} (long-dashed), 3×10^{20} cm^{-3} (dash-dotted), and 2×10^{19} cm^{-3} (dotted) for the STO samples. For the interface, two calculated values (2DEG$_0$) and (2DEG$_{1/2}$) are reported, corresponding to the band structure of the insulating and fully compensated interfaces, respectively. The 2DEG thickness establishing the 2D-3D equivalence is indicated as L_{eq}.

2 nm to 11 nm.[18,20,21,23,29,35] In the STO/LAO calculations, on the other hand, the doping charge Q is fixed in the 3D simulation cell, and n_s is extracted as Q/A; by construction, the thickness is naturally identified with the STO sidelength (2.07 nm) of the simulation supercell, but this is more a constraint rather than an actual determination of L. To bypass this uncertainty, we label each bulk sample with an equivalent thickness $L_{eq} = n_s/n_{3D}$, that is the thickness which establishes the equivalence between bulk STO and STO/LAO samples. Depending on our choice of L, we then select the appropriate bulk to be compared with the interface. Clearly small L is the best-case scenario for larger Seebeck amplitude in 2DEG, while larger L means smaller n_{3D} equivalent to the same n_s; thus larger $|S|$ in bulk. Figure 2 clearly shows that, unless we assume the gas to be extremely localized (with L as small as one or two unit cells), experiment and theory coherently report $|S|$ values larger in STO than in STO/LAO. The main conclusion is a lack of thermopower enhancement at the interface, with respect to the equivalently doped STO bulk.

But which is the reason for this lack of thermopower increase? The thermopower behavior at the interface is hidden in the intricacy of the actual band structure. According to our discussion above, differences between STO/LAO and bulk STO Ti t_{2g} band profile can be rationalized in terms of three specific features: (i) band effective masses, (ii) on-site band offset, and (iii) intersite band offset. The determination of the individual impact of these ingredients is instrumental to a thorough understanding of the thermoelectric behavior. To this aim, we use the effective mass multiband model described in Sec. II which includes 18 bands (6 Ti atoms, consistent with the 2DEG thickness of our *ab initio* calculations, and three t_{2g} orbitals per Ti). In order to highlight the pure confinement effect on the electron charge due to the lowered dimensionality, the relaxation time model parameters are kept equal for the bulk and the interface.

The results for the in-plane component (we fix $j = x$) of Seebeck and electron conductivity are reported in Fig. 3. Total (S_j, σ_j) and band-resolved quantities ($S_{\nu\alpha j}$, $\sigma_{\nu\alpha j}$, where ν and α are Ti-site and orbital indices, respectively) are shown at $T = 100$ K as a function of the total charge of the well $Q = \sum_{\nu\alpha} P_{\nu\alpha}$. The band conductivity $\sigma_{\nu\alpha j}$ increases proportionally to the effective mass prefactor $C_{\nu\alpha j}$, which in turn depends on the inverse of $m*_{\alpha,x}$ (see Sec. II); also, σ increases with the chemical potential μ for two reasons: the Fermi velocity and the relaxation time τ, which both increase with μ. At variance, $S_{\nu\alpha j}$ is proportional to the relative conductivity $\sigma_{\nu\alpha j}/\sigma_j$, and increases in magnitude with decreasing μ.

In the 3D case (upper-most panel of Fig. 3) there is no orbital splitting; all bands are energy-degenerate and equally filled. The difference in band conductivity is only due to the mass prefactor: $C_{d_{xy},x} = C_{d_{xz},x}$, while $C_{d_{yz},x}$ is much smaller since the d_{yz} bands are "heavy" along x; thus $\sigma_{xy,x} = \sigma_{xz,x} \gg \sigma_{yz,x}$. The same order characterizes the band Seebeck coefficients: $S_{xy,x} = S_{xz,x} \gg S_{yz,x}$. In two dimensions (second panel from the top of Fig. 3) the band bottoms are still aligned, but the different masses change the band occupancies: the largest portion of the total charge Q fills the flatter d_{xz} and d_{yz} bands, and only a small portion remains in d_{xy}. For a given Q, the chemical potential μ [and in turn $\tau(\mu)$] is lowered with respect to its 3D value. Total conductivity drops by over an order of magnitude, compared to the 3D value. This has two causes: the decrease of μ and the suppression of the $\sigma_{xy,x}$ band conductivity due to the mass prefactor, since in two dimensions $C_{dxz,x} > C_{d_{xy},x} > C_{d_{yz},x}$. On the contrary, the decrease of μ enhances $|S|$ at small Q from ~ 300 mV/K in three dimensions to ~ 500 mV/K in two dimensions. It is interesting to see how individual bands contribute to this enhancement: the ration $\sigma_{\nu\alpha x}/\sigma_x$ enhances $S_{xz,x}$, which is the dominant contribution, and depresses $S_{xy,x}$, which remains slightly below average. Finally, $S_{yz,x}$ is marginal and similar to the 3D case.

So far the model produces the expected enhancement of S due to the reduced dimensionality. Now we introduce the effect of on-site band splitting (third panel from top of Fig. 3): we add to the 2D bands an on-site homogeneous splitting between singlet d_{xy} and doublet (d_{xz}, d_{yz}) states of $\Delta t_{2g} = 0.1$ eV. This causes a large transfer of charge from d_{xz} and d_{yz} orbitals, which are left nearly empty, into the d_{xy} orbital. The immediate consequence is that μ must shift dramatically upwards, for a given Q, with respect to the degenerate case. Total conductivity

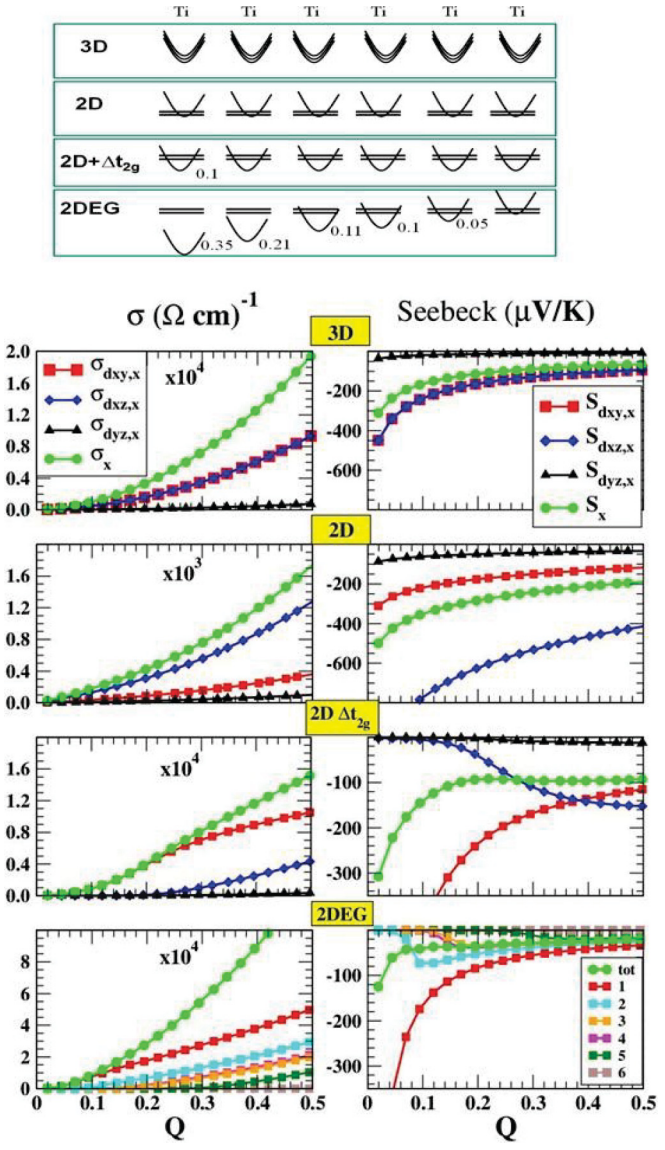

FIG. 3. (Color online) Total and band-by-band t_{2g} conductivity (left panels) and thermopower (right panels) in the x direction as a function of the total charge of the well Q, calculated using the multiband model described in Sec. II C for the cases illustrated schematically in the right panels. From top to bottom: (a) the 3D case; (b) the 2D t_{2g}-degenerate case; (c) the 2D case plus a $d_{xy} - (d_{xz},d_{yz})$ band splitting of 0.1 eV; (d) the 2D case with intersite d_{xy} bands split according to the *ab initio* calculated STO/LAO band structure for $Q = 1/2$.

recovers one order of magnitude with respect to the degenerate case, mainly due to the rise of the d_{xy} contribution. On the other hand, S is brought back to nearly the same value as in three dimensions, thus losing all the advantage gained by the dimensional lowering. Looking at band contributions, $S_{xy,x}$ grows with respect to the t_{2g}-degenerate case, but this gain is largely canceled by the suppression of $S_{xz,x}$, which was the main source of the 2D enhancement.

Finally, in the lowest panel of Fig. 3 we consider a site-dependent, spatially inhomogeneous d_{xy} band offset, mimicking the actual profile of the STO/LAO band structure given by *ab initio* calculations in the case of $Q = 1/2$ electrons per unit area (the marginally occupied d_{xz} and d_{yz} bands are now neglected). Clearly, the intersite band offset favors a charge accumulation into the lowest-energy d_{xy} band on the Ti atom right at the interface (band-1), and the consequent rise of μ. In turn, this causes a fourfold increase in band-1 $\sigma_{xy,x}$ (the red curve of the lowest panel of Fig. 3) and the halving of band-1 $S_{xy,x}$ (red curve of the lowest-right panel) with respect to the on-site split homogeneous case. Since the band Seebeck coefficient is weighted by $\sigma_{xy,x}/\sigma_x$, all other bands add a minor and progressively vanishing contribution to S. Total conductivity σ_x is about five times larger, and the thermopower S_x nearly halved, with respect to their 3D value. This corresponds to a power factor $S^2\sigma$ similar to that of the STO bulk.

In summary, the analysis of STO/LAO shows that the increase in absolute Seebeck coefficient achieved by a pure decrease of dimensionality (which in itself lowers the chemical potential) is overcome by additional features (on-site and intersite band splitting) specific of the interface which increase the chemical potential, thus playing against the rise of thermopower.

IV. DISCUSSION

Measurements and *ab initio* calculations consistently point to a lack of thermopower increase for the 2DEG at the STO/LAO interface. A multiband model used to disentangle conductivity and thermopower in individual band energy contributions provides a simple rationale: the thermopower enhancement due to the 3D-to-2D band mass modification is counteracted by additional on-site and intersite t_{2g} orbital splitting, which both favor the rise of the 2DEG chemical potential, and thus the lowering of the thermopower. Notice that these considerations do not contradict the thermopower rise observed in Nb-doped STO multilayers,[10] since in the latter the negative effects on thermopower discussed for STO/LAO, on-site splitting, and charge accumulation at the interface ultimately due to the large STO/LAO conduction band offset and LAO polarity are expected to occur to a much smaller extent.

This analysis provides a transparent understanding of the thermoelectric behavior of oxide heterostructures, from which simple guidelines can be drawn in the search for oxide heterostructures with improved thermoelectric capabilities. The Seebeck amplitude is largely determined by the chemical potential (measured with respect to the mobility edge energy of the system); thus any band modification, either in terms of band mass or band alignments, enhances (suppresses) the thermopower to the extent that it lowers (increases) the chemical potential. In general, a multiband system possesses more "degrees of freedom" to be potentially exploited to the aim. As an example, the on-site splitting of t_{2g} orbitals is not necessarily detrimental for thermopower: it would actually be advantageous in case the d_{xz}, d_{yz}, and not d_{xy}, were the lowest in energy, since the chemical potential would be lowered.

More generally, any interface characterized by the energy stabilization of the orbitals with larger mass, or, equivalently, by the mass enhancement of the most filled orbitals, is expected to display thermopower enhancement. For what concerns the power factor $S^2\sigma$ the optimal condition is given by highly anisotropic bands, with small masses along the electron current

direction (favoring large σ) and large masses in the orthogonal direction which maximize S.

Finally, we should consider that those simple prescriptions start from the assumption of carriers moving according to the band conductivity regime. However, this may not be sufficient for a full understanding of confinement effects. Recent experiments[12,33,34] indicate the possibility of more complicated scenarios for what concerns transport phenomena in the condition of low doping concentration, possibly related to strong electron correlation. Phenomena such as Mott or Anderson localization, polaronic behavior, and hopping conductivity may have a strong impact and are probably essential to understand the thermoelectric behavior of oxides at low doping. Including these effects in the theoretical description is a nontrivial but necessary direction of development.

V. SUMMARY AND CONCLUSIONS

In summary, measurements and *ab initio* calculations concurrently point to a lack of thermopower increase for the 2DEG confined at the STO/LAO interface, with respect to the equivalent-doped STO bulk. The rationale of this behavior resides in the multiband character of the interface. A parabolic band model based on *ab initio* band energies provides a simple rationale: the thermopower enhancement due to the 3D-to-2D band mass modification is counteracted by additional on-site t_{2g} orbital splitting and intersite band alignment due to charge accumulation at the interface, which both play against the Seebeck enhancement.

These results are not restricted to the case of STO/LAO, but can be usefully applied to the study of thermopower and electric conductivity of any oxide heterostructure. They indicate that the thermopower in low-dimensional oxides can be reliably addressed only by accounting for the specific electronic properties of the system, and suggest possible guidelines for the thermopower optimization.

ACKNOWLEDGMENTS

This work was supported in part by projects EU FP7 *OxIDes* (Grant No. 228989), MIUR-PRIN 2008 *2-DEG FOXI*, IIT Seed *NEWDFESCM*, 5 MiSE-CNR, and Fondazione Banco di Sardegna 2011. M.J.V. acknowledges a visiting professor grant at Cagliari University, the Belgian ARC project TheMoTherm, and a "Crédit d'impulsion" grant from University of Liège. Calculations performed at CASPUR Rome and Cybersar Cagliari.

[1] A. Majumdar, Science **303**, 777 (2004).
[2] M. S. Dresselhaus *et al.*, Adv. Mater. **19**, 1 (2007).
[3] L. D. Hicks and M. S. Dresselhaus, Phys. Rev. B **47**, 12727 (1993); **47**, 16631 (1993); L. D. Hicks *et al.*, *ibid.* **53**, R10493 (1996).
[4] J. O. Sofo and G. D. Mahan, Appl. Phys. Lett. **65**, 2690 (1994); G. D. Mahan and J. O. Sofo, Proc. Natl. Acad. Sci. USA **93**, 7436 (1996).
[5] D. A. Broido and T. L. Reinecke, Phys. Rev. B **51**, 13797 (1995); Appl. Phys. Lett. **67**, 1170 (1995).
[6] T. Koga, X. Sun, S. B. Cronin, and M. S. Dresselhaus, Appl. Phys. Lett. **73**, 2950 (1998); **75**, 2438 (1999); T. Koga *et al.*, Phys. Rev. B **62**, 16703 (2000).
[7] J. Zhou *et al.*, Phys. Rev. Lett. **107**, 226601 (2011).
[8] R. Venkatasubramanian, E. Siivola, T. Colpitts, and B. O'Quinn, Nature (London) **413**, 597 (2001).
[9] T. C. Harman, P. J. Taylor, M. P. Walsh, and B. E. LaForge, Science **297**, 2229 (2002).
[10] H. Ohta *et al.*, Nat. Mater. **6**, 129 (2007); Thin Solid Films **516**, 5916 (2008).
[11] Y. Mune *et al.*, Appl. Phys. Lett. **91**, 192105 (2007).
[12] W. S. Choi *et al.*, Phys. Rev. B **82**, 024301 (2010).
[13] M. L. Scullin *et al.*, Appl. Phys. Lett. **92**, 202113 (2008).
[14] M. Cutler and N. F. Mott, Phys. Rev. **181**, 1336 (1969).
[15] A. Ohtomo and H. Y. Hwang, Nature (London) **427**, 423 (2004).
[16] S. Thiel *et al.*, Science **313**, 1942 (2006).
[17] M. Huijben *et al.*, Nat. Mater. **5**, 556 (2006).
[18] N. Nakagawa *et al.*, Nat. Mater. **5**, 204 (2006).
[19] W. Siemons *et al.*, Phys. Rev. Lett. **98**, 196802 (2007).
[20] M. Basletic *et al.*, Nat. Mater. **7**, 621 (2008).
[21] M. Singh *et al.*, Phys. Rev. Lett. **102**, 176805 (2008).
[22] M. Salluzzo *et al.*, Phys. Rev. Lett. **104**, 166804 (2009).
[23] A. Dubroka *et al.*, Phys. Rev. Lett. **104**, 156807 (2010).
[24] P. R. Willmott *et al.*, Phys. Rev. Lett. **99**, 155502 (2007).
[25] S. A. Pauli *et al.*, Phys. Rev. Lett. **106**, 036101 (2011).
[26] C. Cancellieri, D. Fontaine, S. Gariglio, N. Reyren, A. D. Caviglia, A. Fête, S. J. Leake, S. A. Pauli, P. R. Willmott, M. Stengel, Ph. Ghosez, and J.-M. Triscone, Phys. Rev. Lett. **107**, 056102 (2011).
[27] N. Reyren *et al.*, Science **317**, 1196 (2007).
[28] A. D. Caviglia *et al.*, Nature (London) **456**, 624 (2008).
[29] O. Copie *et al.*, Phys. Rev. Lett. **102**, 216804 (2009).
[30] A. D. Caviglia *et al.*, Phys. Rev. Lett. **104**, 126803 (2010).
[31] A. D. Caviglia *et al.*, Phys. Rev. Lett. **105**, 236802 (2010).
[32] M. Ben Shalom *et al.*, Phys. Rev. Lett. **105**, 206401 (2010).
[33] L. Li *et al.*, Science **332**, 825 (2011).
[34] L. Li *et al.*, Nature Phys. **7**, 762 (2011).
[35] I. Pallecchi *et al.*, Phys. Rev. B **81**, 085414 (2010).
[36] C. Cancellieri *et al.*, Europhys. Lett. **91**, 17004 (2010).
[37] A. Filippetti *et al.*, Phys. Rev. B **84**, 195127 (2011); A. Filippetti and N. A. Spaldin, *ibid.* **67**, 125109 (2003); A. Filippetti and V. Fiorentini, Eur. Phys. J. B **71**, 139 (2009).
[38] P. Delugas *et al.*, Phys. Rev. Lett. **106**, 166807 (2011).
[39] P. B. Allen, in *Quantum Theory of Real Materials*, edited by J. R. Chelikowsky and S. G. Louie (Kluwer, Boston, 1996), pp. 219–250.
[40] G. Madsen and D. Singh, Comput. Phys. Commun. **175**, 67 (2006).
[41] K. Durczewski and M. Ausloos, Phys. Rev. B **61**, 5303 (2000).
[42] T. Okuda *et al.*, Phys. Rev. B **63**, 113104 (2001).
[43] S. Ohta *et al.*, J. Appl. Phys. **97**, 034106 (2005).
[44] H. Usui *et al.*, Phys. Rev. B **81**, 205121 (2011).
[45] J. Mannarth and D. G. Schlom, Science **327**, 1607 (2010).
[46] Z. S. Popovic *et al.*, Phys. Rev. Lett. **101**, 256801 (2008); J.-M. Albina *et al.*, Phys. Rev. B **76**, 165103 (2007); K. Janicka *et al.*, Phys. Rev. Lett. **102**, 106803 (2009); J. Lee *et al.*, Phys. Rev. B **78**, 193104 (2008); R. Pentcheva and W. E. Pickett, *ibid.* **74**, 035112 (2006); W.-J. Son *et al.*, *ibid.* **79**, 245411 (2009); M. Stengel, Phys. Rev. Lett. **106**, 136803 (2011).